CONDENSED MATTER PHYSICS

Controlling the anisotropy of a van der Waals antiferromagnet with light

Dmytro Afanasiev[1,2]*, Jorrit R. Hortensius[1], Mattias Matthiesen[1], Samuel Mañas-Valero[3], Makars Šiškins[1], Martin Lee[1], Edouard Lesne[1], Herre S. J. van der Zant[1], Peter G. Steeneken[1], Boris A. Ivanov[4], Eugenio Coronado[3], Andrea D. Caviglia[1]

Van der Waals magnets provide an ideal playground to explore the fundamentals of low-dimensional magnetism and open opportunities for ultrathin spin-processing devices. The Mermin-Wagner theorem dictates that as in reduced dimensions isotropic spin interactions cannot retain long-range correlations, the long-range spin order is stabilized by magnetic anisotropy. Here, using ultrashort pulses of light, we control magnetic anisotropy in the two-dimensional van der Waals antiferromagnet NiPS₃. Tuning the photon energy in resonance with an orbital transition between crystal field split levels of the nickel ions, we demonstrate the selective activation of a subterahertz magnon mode with markedly two-dimensional behavior. The pump polarization control of the magnon amplitude confirms that the activation is governed by the photoinduced magnetic anisotropy axis emerging in response to photoexcitation of ground state electrons to states with a lower orbital symmetry. Our results establish pumping of orbital resonances as a promising route for manipulating magnetic order in low-dimensional (anti)ferromagnets.

INTRODUCTION

The recent discoveries of van der Waals (vdW) two-dimensional (2D) layered magnets have led to a surge of interest due to their potential applications in constructing atomically thin spin-processing devices and nonvolatile magnetic memories (1, 2). Unique phenomena and effects are foreseen in 2D magnetic systems because of their reduced dimensionality (3). In contrast to 3D magnets, long-range magnetic order cannot exist in 2D at any finite temperature without the presence of magnetic anisotropy (4, 5). In 2D magnets, the anisotropy not only sets a preferred direction for spins but also protects the magnetic order against dimensionality-enhanced thermal spin fluctuations. This intimate relationship between magnetic order and anisotropy in 2D motivates the ongoing search for efficient pathways to manipulate the magnetic anisotropy in such systems. Since the magnetic anisotropy in most materials is determined by the coupling of electronic orbitals and spins, stabilizing and controlling 2D magnetism are actively pursued through the manipulation of orbital degrees of freedom, using, for example, mechanical strain (6–8) and electrostatic gating (9, 10). However, a large anisotropy is normally associated with an unquenched orbital moment, which is limited to specific oxidation states and to low-symmetry crystal environments, most notably for rare-earth ions (11). In most 2D magnets, magnetism arises from transition metal ions, which typically have a quenched orbital moment in their ground state. In these systems, magnetic anisotropy originates from the spin orbit–driven mixing of the ground state with higher-energy orbital states characterized by an unquenched momentum, a rather small effect. Optical pumping of the electronic transitions toward the higher-level orbital states (orbital resonances) provides the most direct access to the admixing and subsequent control of the magnetic anisotropy as manifested

by the excitation of spin precession in 3D magnets (12–15) even to the extent of the subcycle coherent switching of the spin orientation (16–18). Resonant pumping of orbital transitions in 2D magnets, characterized by the subtle interplay between anisotropy and magnetic order, offers unique insights into dynamics of their highly nontrivial elementary excitations, such as, for example, topological magnons (19, 20).

Here, we study resonant optical control of magnetism in nickel phosphorus trisulfide (NiPS₃), a vdW layered magnet with XY-type antiferromagnetism (21–23). The energetic competition between charge transfer and Coulomb repulsion makes this system an intriguing example of a strongly correlated 2D magnet, with pronounced spin-charge correlations (24), spin-orbit entangled excitons (25), and strong spin-lattice coupling (26). We optically pump NiPS₃ using ultrashort pulses of light and probe the ensuing spin dynamics on the picosecond time scale. Continuously varying the pump photon energy across orbital resonances, we identify a transition to the orbital state responsible for the anisotropic magnetic properties in equilibrium. By resonant optical pumping of this transition, we demonstrate the selective activation of a hitherto unreported 2D magnon mode with a terahertz (THz) frequency demonstrating the XY critical scaling with temperature. By studying the mode's excitation as a function of the pump polarization and photon energy, we show that the activation proceeds as a result of the light-induced magnetic anisotropy emerging in response to the resonant photoexcitation of the higher-energy orbital states of Ni²⁺ ions. We also find that optical pumping in the region of optical transparency impulsively activates another high-frequency coherent mode, a previously unreported candidate for the complementary magnon mode in NiPS₃.

RESULTS

NiPS₃ crystallizes in the monoclinic space group C/2m (27) (see Fig. 1A). In the ab plane, it features a network of edge-sharing NiS₆ octahedra arranged on a honeycomb lattice, each having a small

[1]Kavli Institute of Nanoscience, Delft University of Technology, P.O. Box 5046, 2600 GA Delft, Netherlands. [2]Department of Physics, University of Regensburg, Regensburg, Germany. [3]Instituto de Ciencia Molecular (ICMol), Universitat de Valencia Catedrático José Beltrán 2, 46980 Paterna, Spain. [4]Institute of Magnetism, National Academy of Sciences and Ministry of Education and Science, 03142 Kyiv, Ukraine.
*Corresponding author. Email: dmytro.afanasiev@physik.uni-regensburg.de
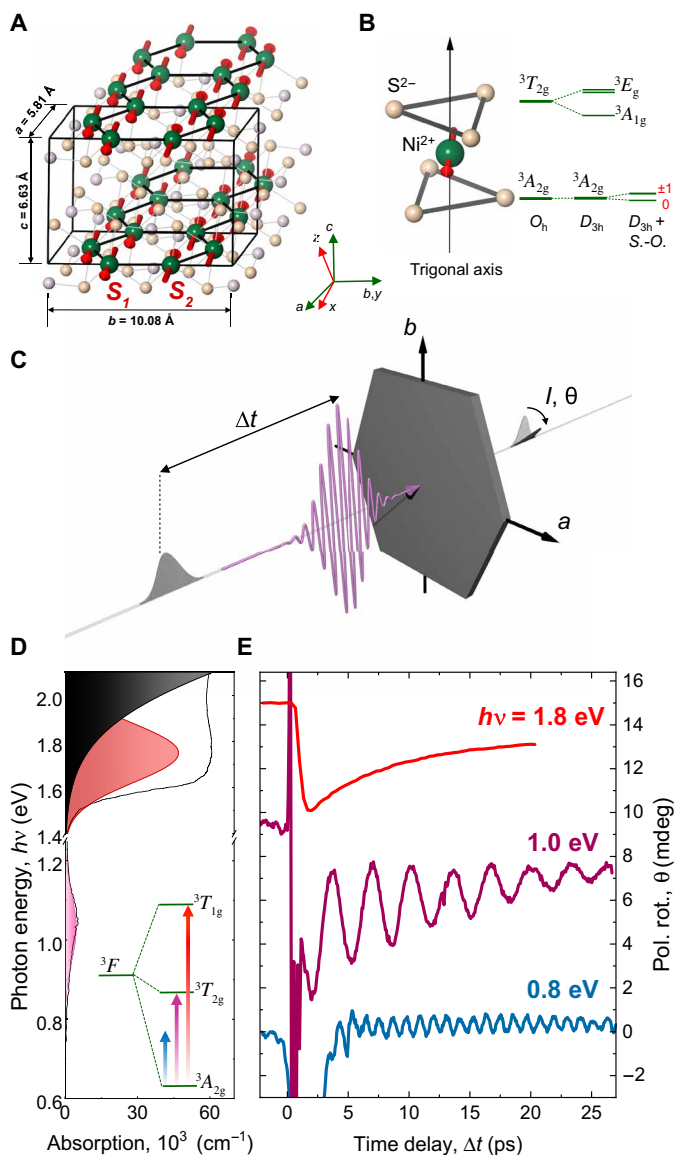
Fig. 1. Ultrafast light-induced dynamics in vdW antiferromagnet NiPS₃.
(**A**) Crystallographic and magnetic structure of NiPS₃. Green/fade orange/light pink spheres represent nickel/sulfur/phosphorous atoms. The green and red triple vectors are crystallographic and magnetic frames, respectively. (**B**) Left: Ni^{2+} ion in the trigonally distorted octahedral sulfide environment. Right: Crystal field splitting of the ground state and first excited triplet state for Ni^{2+} ion (O_h, octahedral field) in a trigonally distorted octahedral environment (D_{3h}); S.-O., spin-orbit coupling. $(0, \pm 1)$ correspond to the projection of the spin moment along the trigonal distortion axis. (**C**) Schematic of the time-resolved pump-probe experiment. The pump (violet) and near-infrared probe (gray) pulses are collinearly focused onto the NiPS₃ sample with variable time delay Δt. The pump-induced dynamics is measured by tracking the pump-induced polarization rotation θ and intensity I of the probe pulses. (**D**) Optical absorption spectrum of NiPS₃ displaying the $^3A_{2g} \rightarrow {}^3T_{2g}$ and $^3A_{2g} \rightarrow {}^3T_{1g}$ absorption bands due to the d-d orbital resonances of Ni^{2+} ions (in pink and red, respectively) and the onset of the above bandgap absorption due to Ni-S charge transfer transitions (black band). (**E**) Experimentally detected polarization rotation signal θ as a function of the delay time Δt after excitation with pump pulses at various photon energies.

trigonal distortion perpendicular to this plane (see Fig. 1B). Below the Néel temperature, $T_N = 155$ K, the magnetic moments of Ni^{2+} ions arrange into a complex compensated antiferromagnetic pattern. The pattern is formed by zigzag ferromagnetic spin chains along the a axis, which are coupled antiferromagnetically within the single layer (*28*) (see Fig. 1A). A large spacing, $c = 6.63$ Å, between adjacent layers leads to a negligible orbital overlap between the magnetic ions of different layers, thereby suppressing interlayer exchange such that the antiferromagnetic order acquires a 2D character already in the bulk form.

The orientation of magnetic moments in NiPS₃ is governed by a biaxial magnetocrystalline anisotropy consisting of two distinct contributions: a dominant easy-plane anisotropy that locks the orientation of the spins to a magnetic plane (xy), slightly inclined from the crystallographic ab plane, and a secondary weaker anisotropy that orients the spins in the magnetic (xy) plane along the x axis. Microscopically, the easy-plane anisotropy develops as a result of a zero-field splitting [$D \approx -1.1$ meV (*29*)] of the $^3A_{2g}$ ground state of the Ni^{2+} ion ($S = 1$) in the crystal field of the trigonally distorted NiS_6 octahedra (see Fig. 1B). Note that $^3A_{2g}$ is an orbital singlet and alone cannot develop the splitting. The splitting and anisotropy arise indirectly as a consequence of spin-orbit–driven intermixing of the ground state with the first excited orbital triplet state $^3T_{2g}$, which is split by the trigonal lattice distortion (*29*, *30*) into a set of low-symmetry doublets ^3E_g and singlets $^3A_{1g}$ separated by an energy gap of around 110 meV, as schematically shown in Fig. 1B. Although there are no reports on the origin of the in-plane magnetic anisotropy along the x axis in NiPS₃, it likely stems from a rhombic distortion of the $NiPS_6$ octahedra, which further splits the $^3A_{2g}$ levels. Hence, an anisotropic Hamiltonian considering not only the axial distortion of the octahedron but also an in-plane distortion may be needed to take this observation into account (see section S6).

The orbital resonances in NiPS₃ correspond to a pair of d-d transitions $^3A_{2g} \rightarrow {}^3T_{2g}$ and $^3A_{2g} \rightarrow {}^3T_{1g}$ emerging within the ^3F ground state multiplet of the Ni^{2+} ion split by the octahedral crystal field (O_h) (see fig. S1). In NiPS₃, these transitions result in a pair of two broad optical absorption bands centered at 1.07 ($^3A_{2g} \rightarrow {}^3T_{2g}$) and 1.73 eV ($^3A_{2g} \rightarrow {}^3T_{1g}$). Note that in contrast to other transition metal ions, the d-d resonances in Ni^{2+} are spin-parity allowed ($\Delta S = 0$), i.e., they do not involve a spin-flip, and thus cannot directly affect the exchange interaction between adjacent spins. To selectively address these resonances, we used ultrashort (~100 fs) pump pulses with photon energy tunable in a broad spectral range of 0.1 to 1.9 eV. The pump-induced dynamics were measured by tracking the intensity I and the rotation of the polarization plane θ of time-delayed copropagating near-infrared probe pulses at a photon energy of 1.55 eV, as schematically shown in Fig. 1C. Whereas I is considered as a measure of the nonmagnetic components of the dielectric tensor, θ is sensitive to the magnetic order via magneto-optical effects, such as the Faraday effect and magnetic linear birefringence.

The sample was cooled down to 10 K, well below T_N, and pumped using linearly polarized pulses at variable photon energies. The time-resolved polarization rotation θ reveals a notable sensitivity of the pump-induced dynamics to the photon energy of the excitation (see Fig. 1, D and E). When excited at the $^3A_{2g} \rightarrow {}^3T_{2g}$ resonance ($h\nu = 1.8$ eV), θ displays a damped oscillation as a function of the pump-probe time delay Δt, with frequency $f_1 = 0.30$ THz (see fig. S2 for the Fourier spectra). No coherent oscillations were observed

when exciting at the higher photon energy ($h\nu = 0.97$ eV) corresponding to the $^3A_{2g} \rightarrow {}^3T_{1g}$ resonance. Detuning the photon energy below the absorption lines of the resonances ($h\nu = 0.8$ eV) shows no signal associated with the frequency f_1 but reveals instead another higher-frequency mode at $f_2 = 0.92$ THz. We note that the oscillations seen in the polarization rotation dynamics were not observed in the probe intensity dynamics I (see fig. S3), thus hinting at their magnetic origin. In addition, we found no match for the frequencies of these oscillations in the phonon spectrum of NiPS$_3$, which was well studied in recent years (26, 31–33).

To understand the significance of the orbital resonances, we tracked the ultrafast dynamics while varying the pump photon energies across the subgap states down to the phonon Reststrahlen band edge at 0.1 eV. The amplitudes of both oscillations at $f_{1,2}$ were retrieved, and their relative values (normalized on the pump fluence) were plotted as a function of the pump photon energy. Figure 2A shows that the f_2 mode is excited in the broad window of optical transparency 0.1 to 0.9 eV, indicating the off-resonant character of the excitation and impulsive stimulated Raman scattering (ISRS) process as a plausible mechanism. In notable contrast, the excitation of the lower-frequency f_1 mode only occurs in a relatively narrow photon energy range, showing a pronounced resonance with the

$^3A_{2g} \rightarrow {}^3T_{2g}$ transitions (see Fig. 2A). The lineshape of the resonance reveals a fine structure indicative of the trigonal splitting of the $^3T_{2g}$ manifold (^3E_g, $^3A_{1g}$) (see fig. S1). Despite a nearly order of magnitude stronger optical absorption, no oscillations were seen upon resonant pumping of the $^3A_{2g} \rightarrow {}^3T_{1g}$ higher-energy orbital resonance, underscoring the exceptional sensitivity of the oscillations to the photoexcitation of the $^3T_{2g}$ states. Whereas the amplitude of the mode at f_2 reveals a linear dependence on the pump fluence (Fig. 2B), the amplitude of the f_1 mode saturates above 5 mJ/cm^2 (Fig. 2C), indicating a possible saturation of the $^3A_{2g} \rightarrow {}^3T_{2g}$ transition.

The temperature (T) dependence of the frequencies $f_{1,2}$ evidences that these modes are sensitive to the magnetic ordering. Figure 3A shows that as T increases, the damping of the first mode goes up, while the frequency f_1 gradually decreases and ultimately converges to zero at a temperature close to T_N. Although the application of a relatively weak in-plane magnetic field H up to 7 kOe produced no observable shift in f_1 (see fig. S4), the observation of the critical softening is a strong indication that the oscillation is of magnetic origin (34, 35). The softening can be characterized by a power law $f_1(T) \propto (T_N - T)^\beta$ (see Fig. 3C and fig. S5), with $T_N \approx 155 \pm 1$ K, in full agreement with literature data, and a critical exponent $\beta = 0.23 \pm 0.01$ valid down to the temperature $T_0 = 0.65\ T_N$ (see fig. S5). Note that the β value also matches remarkably well with the critical exponent of the XY model ($\beta_{XY} = 0.23$) previously proposed to describe the temperature evolution of the 2D magnetic ordering in NiPS$_3$ (36–38). This remarkable observation is an unambiguous and, at the same time, unexpected indication of the intrinsically 2D character of the mode observed in the bulk form of NiPS$_3$.

The temperature evolution of the higher-frequency oscillation at f_2 is substantially different. As T increases, the central frequency f_2 shows a slight increase, which above 75 K is followed by a steep, nearly linear, softening. A linear extrapolation of the frequency decrease versus T suggests that a complete softening of the mode occurs at $T = 170$ K, in proximity to T_N (see Fig. 3D). The softening indicates that the oscillation is either of magnetic origin itself or strongly sensitive to the magnetic ordering. This is further corroborated by the significant growth of the damping constant upon heating. Such highly damped behavior is typical for soft modes in the vicinity of their associated phase transitions (39).

We now analyze the spin dynamics possible in NiPS$_3$ from a phenomenological theory perspective. Two magnon modes are expected in a compensated antiferromagnet, featuring a biaxial magnetic anisotropy (40, 41). The modes correspond to orthogonal deflections of the Néel vector defined as $\mathbf{L} = S(\mathbf{S}_1 - \mathbf{S}_2)$, where $S = S(T)$ is the average value of the Ni^{2+} spin, and $\mathbf{S}_{1,2}$ is a pair of antiferromagnetically coupled spins. In equilibrium, $\mathbf{L}$ is oriented along the x axis, and deflections are expected in ($\parallel$) and out of ($\perp$) the magnetic easy plane (xy), in such a way that the dynamical components ΔL_y and ΔL_z emerge (see Fig. 3, E and F). The frequencies $f_{\parallel,\perp}$ of the magnons are defined by the geometric mean of the respective magnetic anisotropy ($D_{\parallel,\perp}$) and exchange energy J_{ex} (see section S6) and, in addition, proportional to $S(T)$. Hence, both should experience a power-law temperature scaling inherent to the magnetic order parameter $\mathbf{L}$ similarly to the one observed for the f_1 mode. Because the out-of-plane anisotropy is typically more substantial for easy-plane antiferromagnets such as NiPS$_3$, $f_\parallel \ll f_\perp$ is expected. Note that although there is no net magnetization in the ground state: $\mathbf{M} = S(\mathbf{S}_1 + \mathbf{S}_2) = 0$, a finite magnetization component $\mathbf{M} \propto [\dot{\mathbf{L}}, \mathbf{L}]$ emerges due to the dynamics of the Néel vector $\mathbf{L}$ (42). As a consequence, the in- and
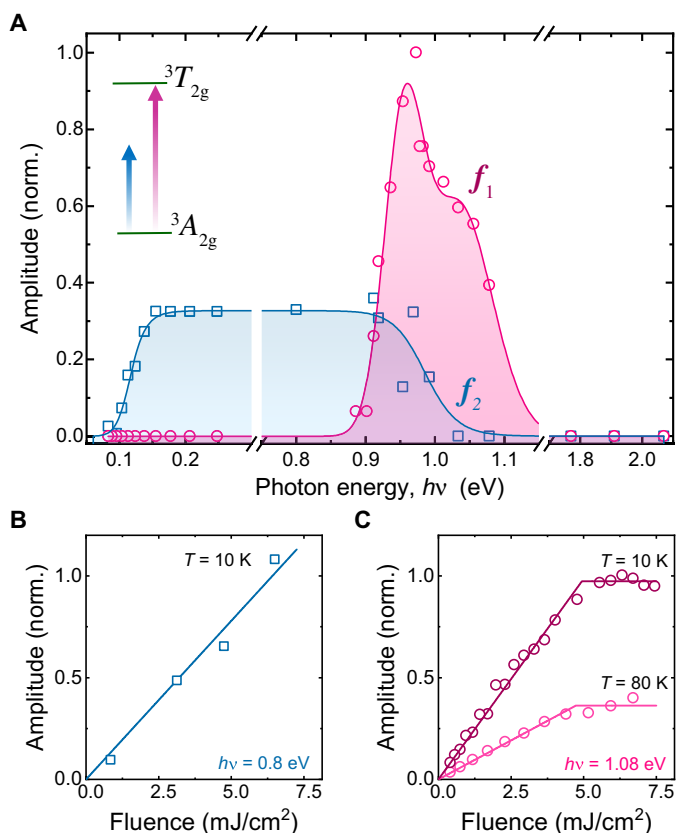

Fig. 2. Selective excitation of the light-induced coherent dynamics. (**A**) Amplitudes of the coherent oscillations corresponding to the modes at frequencies $f_{1,2}$ normalized to the maximal value of the f_1 mode as a function of the pump photon energy. Solid lines are guides to the eye. Inset: Schematic illustration of the optical transition at which the f_1 mode is observed. (**B** and **C**) Amplitude of the oscillation as a function of the pump fluence for the (B) f_2 and (C) f_1 modes. The solid lines are linear fits, including saturation.
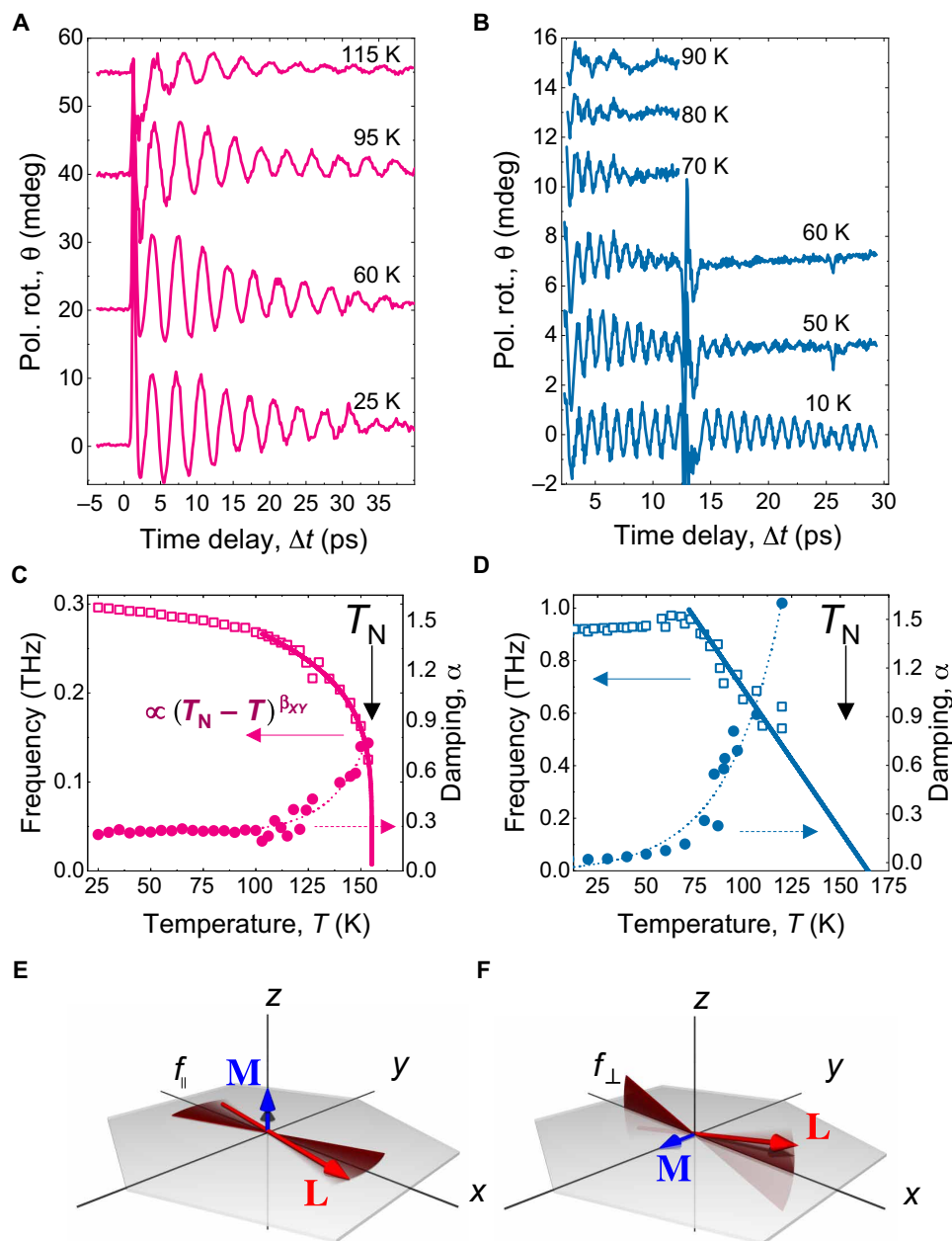
Fig. 3. Critical behavior of the light-induced coherent dynamics. (**A** and **B**) Temperature dependence of the time-resolved polarization rotation after pump-induced excitation with photon energies of 1.08 (A) and 0.2 eV (B). Irregularities at ~13 ps in (B) are related to an artifact of the measurement setup. (**C** and **D**) Frequency (left axis) and damping factor α (right axis) of the oscillations as extracted from the damped sine fits of the time-domain data in (A) and (B). The solid lines represent the best fit of $(T_N - T)^\beta$ (C), which gives $T_N = 155 \pm 1$ K and $\beta = 0.23$, and a linear function (D) to the frequency data. (**E** and **F**) Schematics of the in-plane (E) and out-of-plane (F) magnon modes.

out-of-plane magnetic modes can be fully described by the orthogonal pairs (L_y, M_z) and (L_z, M_y), respectively.

In (43), it was recently shown that the application of an in-plane magnetic field larger than $H_{sf} = 100$ kG promotes a spin-flop transition in NiPS$_3$, during which the spins suddenly rotate in the easy-plane and, in addition, cant along the field orientation. It can be easily shown (see section S7) that the magnitude of the spin-flop field H_{sf} is a direct measure of the frequency of the in-plane dynamics $f_\parallel = \gamma H_{sf} = 280$ GHz, where $\gamma = 28 \cdot 10^{-4}$ GHz/G is the

gyromagnetic ratio. This estimate agrees particularly well with f_1 and thus provides another strong indication that the coherent oscillation excited upon resonant pumping of the $^3A_{2g} \rightarrow {}^3T_{2g}$ transition is the in-plane magnon mode characterized by L_y and M_z and a 2D critical scaling. We note that even though there is an oscillating out-of-plane magnetic component M_z, the experimentally observed oscillations show a strong phase and amplitude dependence on the orientation of the probe polarization plane with respect to the crystal axes, indicating that the detection of this mode is given by

linear magnetic birefringence due to the L_y component rather than Faraday rotation, sensitive to M_z (44).

Having identified $f_\parallel = f_1$, we put forward the assumption that the higher-frequency oscillation at f_2 can be assigned to the complementary out-of-plane magnon ($f_\perp = f_2$). Our phenomenological theory (see section S8) suggests that excitation of the out-of-plane magnon mode with linearly polarized light is possible in NiPS$_3$ due to the low-symmetry (monoclinic) distortion of the crystal lattice. However, these assumptions do not agree with the recently reported, although mutually conflicting, values for the zone-center magnon at the significantly higher frequencies of 1.69 and 2.4 THz from (45) and (25), respectively. To unambiguously establish the origin of the coherent mode f_2, time-resolved measurements in high magnetic fields, $H \geq H_{\mathrm{sf}}$, are of primary importance.

To further our understanding of the excitation mechanism of the in-plane (f_1) magnon and its relation to the light-induced magnetic anisotropy, we varied the orientation of the pump polarization plane, set by the azimuthal angle ϕ (see Fig. 4A). Although the optical absorption at the $^3A_{2g} \rightarrow {}^3T_{2g}$ orbital resonance is nearly independent of ϕ, the amplitude and phase of the induced magnetic oscillations are strongly affected by variation of the angle. Figure 4B shows that the amplitude of the excited magnon follows a clear π-periodic sinusoid with maxima corresponding to the polarization

oriented at ±45° with respect to the orientation of the Néel vector **L**. This dependency can be simply understood: The linearly polarized light incident at normal to the (ab) crystal plane promptly induces a magnetic anisotropy axis, directed along the orientation of the pump polarization plane. The axis breaks the magnetic symmetry in the basal plane (xy), providing an in-plane magnetic torque sufficiently short to impulsively trigger the planar motion of the spins (see Fig. 4C). The validity of this scenario is further supported by a phenomenological theory based on symmetry considerations and general principles of light-matter interactions in a magnetic medium (see section S8).

DISCUSSION

The azimuthal dependence of the oscillation amplitude on the orientation of the pump polarization allows us to attribute the excitation of the in-plane magnon mode to an ultrafast light-induced change of the magnetocrystalline anisotropy. This anisotropy emerges in response to resonant optical excitation of the Ni^{2+} electrons to the $^3T_{2g}$ orbital state, characterized by an unquenched net angular momentum. To estimate the lifetime of the photoinduced anisotropy, we performed a time-resolved analysis of the frequency of the spin precession at various fluences of the incident pump. A long-living
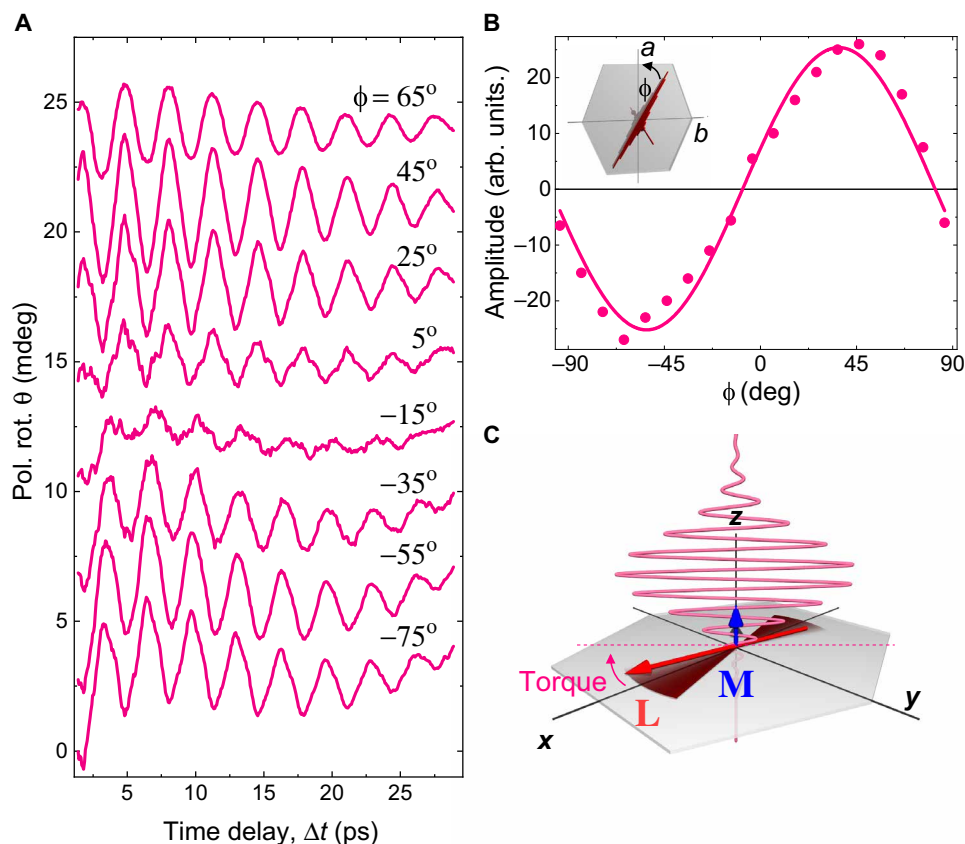

Fig. 4. Selection rules for the excitation of the in-plane magnetic mode. (**A**) Pump-induced rotation of the probe polarization plane as a function of pump-probe delay time Δt for different orientations of the linear polarization of the pump. The pump photon energy is 1.0 eV. (**B**) The amplitude of the oscillations as a function of the azimuthal angle ϕ between the pump polarization plane and the a crystal axis. (**C**) Schematics showing that the electric field of light acts as an instantaneous photomagnetic anisotropy (dashed line) with a direction along the light polarization plane, resulting in a torque and subsequent oscillations of the Néel vector **L** and net magnetization **M**.

change in the anisotropy should renormalize the magnon frequency within the lifetime of the excited state in agreement with (46, 47) and the derived formulas in sections S6 and S8 and thus can be seen as a measure of the magnetic anisotropy relaxation. Consequently, exciting with greater fluence would amplify this effect: The spin precession frequency would scale with the fluence. In contradiction to this, we observe that fluence affects only the amplitude but not the frequency of the spin precession (fig. S9), which indicates that the lifetime of the anisotropy is at least shorter than the period of the spin precession (<3 ps). The short lifetime of the anisotropy can originate from the short-lived photoexcited state, whose lifetime is given by the natural width of the $^3A_{2g} \rightarrow {}^3T_{2g}$ absorption line (0.2 eV) and is on the order of 20 fs. The observed polarization control of the spin precesion is strongly reminiscent of the inverse Cotton-Mouton effect (48), a particular variant of the magnetic ISRS also widely considered as an instantaneous photoinduced magnetic anisotropy (49, 50). In the magnetic ISRS scenario, the pump photon is scattered in an event where an electron momentarily gains orbital angular momentum from the higher-level orbital states typically having energy higher than the incident photon. Our experimental results can thus be interpreted alternatively as being indicative of the resonant enhancement of the scattering process upon approaching the transition to the higher-level $^3T_{2g}$ orbital state, underlining the strong impact of the low-symmetry trigonal $^3T_{2g}$ states on the magnetic anisotropy of $NiPS_3$. Several works reported that magnetic ISRS processes in iron-based compounds can be significantly enhanced in the vicinity of the d-d transitions [see, for example, (14, 15)]. Our experiment shows that almost no magnon excitation is observed for the photon energies below the $^3A_{2g} \rightarrow {}^3T_{2g}$ resonance, contrary to what is expected for the ISRS process. The resonant enhancement picture must thus assume that the magnon amplitude falls below our detection limit away from the resonance. Regardless of the exact microscopic nature of the driving mechanism, we emphasize the crucial role of the d-d transitions for optical control of magnetic anisotropy in $NiPS_3$.

In conclusion, our work establishes selective pumping of orbital resonances as an efficient pathway to control magnetic anisotropy and to reveal high-frequency 2D coherent spin dynamics in vdW layered antiferromagnets. While ultrafast control of the magnetic anisotropy and sub-THz spin dynamics is demonstrated here, in bulk lamellar $NiPS_3$, due to advances in exfoliating techniques and strong magneto-optical responses observed in our experiments, we anticipate the applicability of the suggested approach to atomically thin antiferromagnets (26, 51). Such systems can serve as an excellent test bed for the theoretical XY model, with further possibilities such as revealing dynamics of nontrivial topological vortex states associated with the Berezinskii-Kosterlitz-Thouless transition (3, 26).

MATERIALS AND METHODS
Crystals of $NiPS_3$ were grown by chemical vapor transport. First, polycrystalline $NiPS_3$ was synthesized by mixing powders of S (99.998%, from Sigma-Aldrich), P (> 99.99%, from Sigma-Aldrich), and Ni (99.99%, from Sigma-Aldrich) in a stoichiometric ratio, pressed into a pellet, and sealed in a quartz ampoule (P $\sim 5 \cdot 10^{-5}$ mbar, length = 25 cm, internal diameter = 1.5 cm). The ampoule was kept at 400°C for 20 days and cooled down slowly (0.07°C/min). Next, the previous material was mixed with iodine (99.999% anhydrous beads from Sigma-Aldrich; $[I_2] \sim 5$ mg/cm^3), sealed in

an evacuated quartz ampoule (P $\sim 5 \cdot 10^{-5}$ mbar, length = 50 cm, internal diameter = 1.5 cm), and placed in a three-zone furnace in a gradient of temperatures of 700°/650°/675°C for 28 days. Phase and compositional purity were verified by powder x-ray diffraction and inductively coupled plasma optical emission spectrometry. The materials were handled inside an argon glove box to avoid any possible oxidation. Exact details about temperature gradients and characterization of crystals from the same batch as the ones used in this work can be found in (6).

The pump pulses at the photon energies of 0.8 to 1.9 eV (~100 fs) were obtained using an optical parametric amplifier (OPA), and to access energies below 0.4 eV (~200 fs), we used difference frequency generation by mixing the outputs of two OPAs in a GaSe crystal (52). The pump pulses at a 500-Hz repetition rate were focused on the sample surface to a spot with a diameter of 200 μm. The time-delayed copropagating near-infrared probe pulses at a photon energy of 1.55 eV were focused to a spot of 130 μm, such that the spatial overlap between pump and probe pulses was satisfied.

SUPPLEMENTARY MATERIALS

REFERENCES AND NOTES
1. Y. Khan, S. M. Obaidulla, M. R. Habib, A. Gayen, T. Liang, X. Wang, M. Xu, Recent breakthroughs in two-dimensional van der Waals magnetic materials and emerging applications. *Nano Today* **34**, 100902 (2020).
2. M. C. Wang, C. C. Huang, C. H. Cheung, C. Y. Chen, S. G. Tan, T. W. Huang, Y. Zhao, Y. Zhao, G. Wu, Y.-P. Feng, H.-C. Wu, C.-R. Chang, Prospects and opportunities of 2D van der Waals magnetic systems. *Ann. Phys.* **532**, 1900452 (2020).
3. K. S. Burch, D. Mandrus, J.-G. Park, Magnetism in two-dimensional van der Waals materials. *Nature* **563**, 47–52 (2018).
4. B. Huang, G. Clark, E. Navarro-Moratalla, D. R. Klein, R. Cheng, K. L. Seyler, D. Zhong, E. Schmidgall, M. A. McGuire, D. H. Cobden, W. Yao, D. Xiao, P. Jarillo-Herrero, X. Xu, Layer-dependent ferromagnetism in a van der Waals crystal down to the monolayer limit. *Nature* **546**, 270–273 (2017).
5. C. Gong, L. Li, Z. Li, H. Ji, A. Stern, Y. Xia, T. Cao, W. Bao, C. Wang, Y. Wang, Z. Q. Qiu, R. J. Cava, S. G. Louie, J. Xia, X. Zhang, Discovery of intrinsic ferromagnetism in two-dimensional van der Waals crystals. *Nature* **546**, 265–269 (2017).
6. M. Šiškins, M. Lee, S. Mañas-Valero, E. Coronado, Y. M. Blanter, H. S. van der Zant, P. G. Steeneken, Magnetic and electronic phase transitions probed by nanomechanical resonators. *Nat. Commun.* **11**, 2698 (2020).
7. Y. Sun, R. C. Xiao, G. T. Lin, R. R. Zhang, L. S. Ling, Z. W. Ma, X. Luo, W. J. Lu, Y. P. Sun, Z. G. Sheng, Effects of hydrostatic pressure on spin-lattice coupling in two-dimensional ferromagnetic $Cr_2Ge_2Te_6$. *Appl. Phys. Lett.* **112**, 072409 (2018).
8. Y. Wang, C. Wang, S. J. Liang, Z. Ma, K. Xu, X. Liu, L. Zhang, A. S. Admasu, S. W. Cheong, L. Wang, M. Chen, Z. Liu, B. Cheng, W. Ji, F. Miao, Strain-sensitive magnetization reversal of a van der Waals magnet. *Adv. Mater.*, 2004533 (2020).
9. B. Huang, G. Clark, D. R. Klein, D. MacNeill, E. Navarro-Moratalla, K. L. Seyler, N. Wilson, M. A. McGuire, D. H. Cobden, D. Xiao, W. Yao, P. Jarillo-Herrero, X. Xu, Electrical control of 2D magnetism in bilayer CrI_3. *Nat. Nanotechnol.* **13**, 544–548 (2018).
10. Z. Wang, T. Zhang, M. Ding, B. Dong, Y. Li, M. Chen, X. Li, J. Huang, H. Wang, X. Zhao, Y. Li, D. Li, C. Jia, L. Sun, H. Guo, Y. Ye, D. Sun, Y. Chen, T. Yang, J. Zhang, S. Ono, Z. Han, Z. Zhang, Electric-field control of magnetism in a few-layered van der Waals ferromagnetic semiconductor. *Nat. Nanotechnol.* **13**, 554–559 (2018).
11. K. Yosida, The status of the theories of magnetic anisotropy. *J. Appl. Phys.* **39**, 511–518 (1968).
12. R. V. Mikhaylovskiy, T. J. Huisman, A. I. Popov, A. K. Zvezdin, T. H. M. Rasing, R. V. Pisarev, A. V. Kimel, Terahertz magnetization dynamics induced by femtosecond resonant pumping of Dy^{3+} subsystem in the multisublattice antiferromagnet $DyFeO_3$. *Phys. Rev. B* **92**, 094437 (2015).
13. S. Baierl, M. Hohenleutner, T. Kampfrath, A. K. Zvezdin, A. V. Kimel, R. Huber, R. V. Mikhaylovskiy, Nonlinear spin control by terahertz-driven anisotropy fields. *Nat. Photonics* **10**, 715–718 (2016).
14. R. Iida, T. Satoh, T. Shimura, K. Kuroda, B. A. Ivanov, Y. Tokunaga, Y. Tokura, Spectral dependence of photoinduced spin precession in $DyFeO_3$. *Phys. Rev. B* **84**, 064402 (2011).

15. R. V. Mikhaylovskiy, T. J. Huisman, V. A. Gavrichkov, S. I. Polukeev, S. G. Ovchinnikov, D. Afanasiev, R. V. Pisarev, T. Rasing, A. V. Kimel, Resonant pumping of *d-d* crystal field electronic transitions as a mechanism of ultrafast optical control of the exchange interactions in iron oxides. *Phys. Rev. Lett.* **125**, 157201 (2020).

16. A. Stupakiewicz, K. Szerenos, D. Afanasiev, A. Kirilyuk, A. V. Kimel, Ultrafast nonthermal photo-magnetic recording in a transparent medium. *Nature* **542**, 71–74 (2017).

17. S. Schlauderer, C. Lange, S. Baierl, T. Ebnet, C. P. Schmid, D. C. Valovcin, A. K. Zvezdin, A. V. Kimel, R. V. Mikhaylovskiy, R. Huber, Temporal and spectral fingerprints of ultrafast all-coherent spin switching. *Nature* **569**, 383–387 (2019).

18. A. Stupakiewicz, K. Szerenos, M. D. Davydova, K. A. Zvezdin, A. K. Zvezdin, A. Kirilyuk, A. V. Kimel, Selection rules for all-optical magnetic recording in iron garnet. *Nat. Commun.* **10**, 612 (2019).

19. E. V. Boström, M. Claassen, J. W. McIver, G. Jotzu, A. Rubio, M. A. Sentef, Light-induced topological magnons in two-dimensional van der Waals magnets. *SciPost Phys.* **9**, 061 (2020).

20. X.-X. Zhang, L. Li, D. Weber, J. Goldberger, K. F. Mak, J. Shan, Gate-tunable spin waves in antiferromagnetic atomic bilayers. *Nat. Mater.* **19**, 838–842 (2020).

21. M. Coak, D. Jarvis, H. Hamidov, C. Haines, P. Alireza, C. Liu, S. Son, I. Hwang, G. Lampronti, D. Daisenberger, Tuning dimensionality in van-der-Waals antiferromagnetic Mott insulators TM*P*S₃. *J. Phys. Condens. Matter* **32**, 124003 (2019).

22. F. Wang, T. A. Shifa, P. Yu, P. He, Y. Liu, F. Wang, Z. Wang, X. Zhan, X. Lou, F. Xia, J. He, New frontiers on van der Waals layered metal phosphorous trichalcogenides. *Adv. Funct. Mater.* **28**, 1802151 (2018).

23. K.-Z. Du, X.-z. Wang, Y. Liu, P. Hu, M. I. B. Utama, C. K. Gan, Q. Xiong, C. Kloc, Weak van der Waals stacking, wide-range band gap, and Raman study on ultrathin layers of metal phosphorus trichalcogenides. *ACS Nano* **10**, 1738–1743 (2016).

24. S. Y. Kim, T. Y. Kim, L. J. Sandilands, S. Sinn, M.-C. Lee, J. Son, S. Lee, K.-Y. Choi, W. Kim, B.-G. Park, C. Jeon, H. D. Kim, C. H. Park, J. G. Park, S. J. Moon, T. W. Noh, Charge-spin correlation in van der Waals antiferromagnet NiPS₃. *Phys. Rev. Lett.* **120**, 136402 (2018).

25. S. Kang, K. Kim, B. H. Kim, J. Kim, K. I. Sim, J.-U. Lee, S. Lee, K. Park, S. Yun, T. Kim, A. Nag, A. Walters, M. Garcia-Fernandez, J. Li, L. Chapon, K.-J. Zhou, Y.-W. Son, J. H. Kim, H. Cheong, J.-G. Park, Coherent many-body exciton in van der Waals antiferromagnet NiPS₃. *Nature* **583**, 785–789 (2020).

26. K. Kim, S. Y. Lim, J.-U. Lee, S. Lee, T. Y. Kim, K. Park, G. S. Jeon, C.-H. Park, J.-G. Park, H. Cheong, Suppression of magnetic ordering in XXZ-type antiferromagnetic monolayer NiPS₃. *Nat. Commun.* **10**, 345 (2019).

27. R. Brec, Review on structural and chemical properties of transition metal phosphorus trisulfides MPS₃, in *Intercalation in Layered Materials* (Springer, 1986), pp. 93–124.

28. A. R. Wildes, V. Simonet, E. Ressouche, G. J. Mcintyre, M. Avdeev, E. Suard, S. A. Kimber, D. Lançon, G. Pepe, B. Moubaraki, Magnetic structure of the quasi-two-dimensional antiferromagnet NiPS₃. *Phys. Rev. B* **92**, 224408 (2015).

29. P. A. Joy, S. Vasudevan, Magnetism in the layered transition-metal thiophosphates MPS₃(*M*=Mn, Fe, and Ni). *Phys. Rev. B* **46**, 5425–5433 (1992).

30. N. Chandrasekharan, S. Vasudevan, Magnetism and exchange in the layered antiferromagnet NiPS₃. *J. Phys. Condens. Matter* **6**, 4569 (1994).

31. M. Bonilla, S. Kolekar, Y. Ma, H. C. Diaz, V. Kalappattil, R. Das, T. Eggers, H. R. Gutierrez, M.-H. Phan, M. Batzill, Strong room-temperature ferromagnetism in VSe₂ monolayers on van der Waals substrates. *Nat. Nanotechnol.* **13**, 289–293 (2018).

32. K. Kim, J.-U. Lee, H. Cheong, Raman spectroscopy of two-dimensional magnetic van der Waals materials. *Nanotechnology* **30**, 452001 (2019).

33. A. Hashemi, H.-P. Komsa, M. Puska, A. V. Krasheninnikov, Vibrational properties of metal phosphorus trichalcogenides from first-principles calculations. *J. Phys. Chem. C* **121**, 27207–27217 (2017).

34. J. Nishitani, K. Kozuki, T. Nagashima, M. Hangyo, Terahertz radiation from coherent antiferromagnetic magnons excited by femtosecond laser pulses. *Appl. Phys. Lett.* **96**, 221906 (2010).

35. J. Nishitani, T. Nagashima, M. Hangyo, Terahertz radiation from antiferromagnetic MnO excited by optical laser pulses. *Appl. Phys. Lett.* **103**, 081907 (2013).

36. A. Taroni, S. T. Bramwell, P. C. Holdsworth, Universal window for two-dimensional critical exponents. *J. Phys. Condens. Matter* **20**, 275233 (2008).

37. S. T. Bramwell, P. C. W. Holdsworth, Magnetization: A characteristic of the Kosterlitz-Thouless-Berezinskii transition. *Phys. Rev. B* **49**, 8811–8814 (1994).

38. S. T. Bramwell, P. C. W. Holdsworth, Magnetization and universal sub-critical behaviour in two-dimensional XY magnets. *J. Phys. Condens. Matter* **5**, L53 (1993).

39. J. F. Scott, Soft-mode spectroscopy: Experimental studies of structural phase transitions. *Rev. Mod. Phys.* **46**, 83–128 (1974).

40. S. M. Rezende, A. Azevedo, R. L. Rodríguez-Suárez, Introduction to antiferromagnetic magnons. *J. Appl. Phys.* **126**, 151101 (2019).

41. B. A. Ivanov, Mesoscopic antiferromagnets: Statics, dynamics, and quantum tunneling (Review). *Low Temp. Phys.* **31**, 635–667 (2005).

42. E. G. Galkina, B. A. Ivanov, Dynamic solitons in antiferromagnets (Review Article). *Low Temp. Phys.* **44**, 618–633 (2018).

43. X. Wang, J. Cao, Z. Lu, A. Cohen, H. Kitadai, T. Li, Q. Tan, M. Wilson, C. H. Lui, D. Smirnov, S. Sharifzadeh, X. Ling, Spin-induced linear polarization of photoluminescence in antiferromagnetic van der Waals crystals. *Nat. Mater.* (2021), https://doi.org/10.1038/s41563-021-00968-7.

44. G. A. Smolenskiĭ, R. V. Pisarev, I. Siniĭ, Birefringence of light in magnetically ordered crystals. *Sov. Phys. Usp.* **18**, 410–429 (1975).

45. D. Lançon, R. A. Ewings, T. Guidi, F. Formisano, A. R. Wildes, Magnetic exchange parameters and anisotropy of the quasi-two-dimensional antiferromagnet NiPS₃. *Phys. Rev. B* **98**, 134414 (2018).

46. D. Afanasiev, J. R. Hortensius, B. A. Ivanov, A. Sasani, E. Bousquet, Y. M. Blanter, R. V. Mikhaylovskiy, A. V. Kimel, A. D. Caviglia, Ultrafast control of magnetic interactions via light-driven phonons. *Nat. Mater.* **20**, 607–611 (2021).

47. F. Atoneche, A. M. Kalashnikova, A. V. Kimel, A. Stupakiewicz, A. Maziewski, A. Kirilyuk, T. Rasing, Large ultrafast photoinduced magnetic anisotropy in a cobalt-substituted yttrium iron garnet. *Phys. Rev. B* **81**, 214440 (2010).

48. A. M. Kalashnikova, A. V. Kimel, R. V. Pisarev, V. N. Gridnev, A. Kirilyuk, T. Rasing, Impulsive generation of coherent magnons by linearly polarized light in the easy-plane antiferromagnet FeBO₃. *Phys. Rev. Lett.* **99**, 167205 (2007).

49. A. M. Kalashnikova, A. V. Kimel, R. V. Pisarev, Ultrafast opto-magnetism. *Phys. Usp.* **58**, 969–980 (2015).

50. D. Bossini, T. Rasing, Femtosecond optomagnetism in dielectric antiferromagnets. *Phys. Scr.* **92**, 024002 (2017).

51. C.-T. Kuo, M. Neumann, K. Balamurugan, H. J. Park, S. Kang, H. W. Shiu, J. H. Kang, B. H. Hong, M. Han, T. W. Noh, J.-G. Park, Exfoliation and Raman spectroscopic fingerprint of few-layer NiPS₃ van der Waals crystals. *Sci. Rep.* **6**, 20904 (2016).

52. F. Junginger, A. Sell, O. Schubert, B. Mayer, D. Brida, M. Marangoni, G. Cerullo, A. Leitenstorfer, R. Huber, Single-cycle multiterahertz transients with peak fields above 10 MV/cm. *Opt. Lett.* **35**, 2645–2647 (2010).